A Joint Variational Model for Atmospheric Distortion Correction *

Melissa Y. Tong, Jérôme Gilles, and Luminita A. Vese

Revised August, 2019

Geffen Academy at UCLA
Department of Mathematics and Statistics, San Diego State University
Department of Mathematics, University of California, Los Angeles

Abstract

We study the problem of restoring images distorted by atmospheric turbulence. Geometric distortions and blur are thetwo main components of degradations due to atmospheric turbulence, and prior work has been done to address thesecomponents separately. We propose a joint variational deblurring and geometric distortion correction model and presentnumerical results on synthetic and real data.

1 Introduction and Background

Atmospherically-distorted images of a static scene arise in long range imaging where the images are distorted by turbulent geometric distortion and blurring effects during their acquisition. A model for this degradation is presented in Frakes et. al. [2, 4]

$$f_i(x) = \Phi_i(K(u(x))) + \text{noise}, \tag{1}$$

where a static undistorted scene $u(x)$ is distorted with blurring effects modeled by blur kernel K and geometric distortion effects represented by the operator Φ_i to yield respective distorted frames f_i. The goal is to recover the static scene u from a stream of distorted image frames of the static scene.

In the model of turbulence (1), the distorted image f_i is generated by first blurring the static image u and then degrading the resulting blurry image with geometric distortions. The authors of [7] study both this case and the case where the static image is first affected with geometric distortions and then with blur (i.e. $f_i(x) = K(\Phi_i(u(x))) + \text{noise}$). In their work, they use temporal filtering in combination with registration to correct for geometric distortions and a blind deconvolution algorithm to correct for blurring effects.

*This work was supported in part by NSF Expeditions in Computing Award CCF-0926127 and NSF-DMS Award 0714945.

In the work [9], the authors formulate blind image deconvolution as a principal components analysis (PCA) problem, and they perform restoration experiments on atmospheric turbulence-degraded imagery. Whereas in [15], the focus is more on geometric distortion correction. The authors use a Kalman filter to recover the static scene from a series of distorted frames. They assume a high frame rate and use time-dependent differential equations to model the warping of the frames.

In a different type of approach, the authors of [1] present an improved "lucky-region" fusion (LRF) approach. The LRF approach estimates the local quality of images using an image quality map, which is often based on the gradient of the image. The image quality map selects the best quality regions of each image, and these "lucky-regions" are fused together to give the restored static image.

In a very recent work [10], the authors propose a method that performs joint frame sharpening with the Sobolev gradient method and temporal distortion correction using the Laplace operator. With the reconstructed frames, they apply an approach similar to the lucky-region fusion approach to reconstruct the static image.

In the work [11], the authors address specifically the geometric distortions caused by atmospheric turbulence. They start with a reference frame that is a good approximation of the static scene (usually the mean of the input frames) and estimate the optical flows from this reference frame to each of the input frames. Once the optical flows are determined, they are used to determine a new reference frame, where this new reference frame is the solution of a variational problem involving nonlocal TV regularization. Once this new reference frame is found, the process repeats. A geometrically corrected image results after a few iterations of this process.

A recent approach to deblur the effects of atmospheric turbulence is proposed in [8], where the authors utilize the Fried kernel [3] in a framelet based deconvolution algorithm. The Fried kernel is an analytical formulation of the atmosphere modulation transfer function (MTF) and depends on parameters of the acquisition system and characteristics of the imaging scene as well as a refractive index structure which reflects the turbulence level in the atmosphere. In their work, a method to estimate this refractive index structure parameter is provided. In the next section, we give a brief review of the Fried kernel.

The last two prior works have been combined to produce very nice results. First, the input frames are used to produce a geometrically corrected image using [11]. The geometrically corrected result is then used as input for the deconvolution algorithm in [8]. This two step process yields a deblurred and geometrically corrected image. Our goal is to combine both the deconvolution and geometric correction into one variational restoration model. We give preliminary results for this model.

1.1 Review of Fried Kernel

We give here the basic form of the MTF of the Fried kernel to illustrate its behavior as a function of four parameters D, L, λ, and C_n^2. For more details, we refer the reader to [3, 8]. In two dimensions, letting ω be the frequency modulus, Fried's MTF $M_F(\omega)$ (in the Fourier domain) is given by

$$M_F(\omega) = M_0(\omega) M_{\mathrm{SA}}(\omega) \tag{2}$$

where

$$M_0(\omega) = \begin{cases} \frac{2}{\pi}(\arccos(\omega) - \omega\sqrt{1-\omega^2}) & \text{for } \omega < 1 \\ 0 & \text{for } \omega > 1, \end{cases} \tag{3}$$

and

$$M_{\mathrm{SA}}(\omega) = \exp\left\{ - (2.1X)^{5/3}(\omega^{5/3} - V(Q,X)\omega^2)\right\}. \tag{4}$$

$k = \frac{2\pi}{\lambda}$, $r_0 = 2.1\rho_0 = 2.1(1.437(k^2 L C_n^2))^{-3/5}$, $Q = \frac{D}{\sqrt{\lambda L}}$, $X = \frac{D}{r_0}$, and

$$V(Q,X) = \mathrm{A}(Q) + \frac{\mathrm{B}(Q)}{10}\exp\left\{ - \frac{(\log_{10}(X)+1)^3}{3.5}\right\} \tag{5}$$

where A and B depend on Q only.

Here, D is the system entrance pupil diameter, L is the path length given by the distance between the sensor and acquired scene, λ is the wavelength on which the imaging system is working, and C_n^2 is the refractive index structure reflecting the turbulence level of the atmosphere (for more information on C_n^2, we refer the reader to [16]). As measured in [16], C_n^2 is typically in the range $[10^{-16}m^{-2/3}, 10^{-12}m^{-2/3}]$ where larger values of C_n^2 correspond to stronger turbulence.

1.2 Geometric Distortion Operator and Computation of Its Adjoint

For the notation of the geometric distortion operator and the computation of its adjoint, we follow the notations and method presented in [11]. Let $g = g(x_1, x_2)$, $v_1 = v_1(x_1, x_2)$ and $v_2 = v_2(x_1, x_2)$ be functions from $\mathbb{R}^2$ to $\mathbb{R}$. We define the geometric distortion operator Φ by

$$\Phi : g(x_1, x_2) \to g(x_1 + v_1(x_1, x_2), x_2 + v_2(x_1, x_2)). \tag{6}$$

For fixed v_1 and v_2, Φ is a linear operator on the space of functions from $\mathbb{R}^2$ to $\mathbb{R}$.

The adjoint of Φ is denoted Φ^T and is defined as the operator such that

$$\langle h, \Phi^T g\rangle = \int h(\Phi^T g)dx = \int (\Phi h) g dx = \langle \Phi h, g\rangle \quad \forall h. \tag{7}$$

Numerically, the authors of [11] take h in (7) to be the 'single spike function'

$$h_y(x) = \begin{cases} 1 & \text{if } y = x \\ 0 & \text{if } y \neq x, \end{cases} \tag{8}$$

and subsequently arrive at the relation

$$(\Phi^T g)(y) = \langle h_y, \Phi^T g\rangle = \langle \Phi h_y, g\rangle. \tag{9}$$

$\langle \Phi h_y, g\rangle$ is easy to evaluate since Φh_y is a simple function.

2 Proposed Variational Model

We propose two variations of a combined deblurring and geometric distortion correction model. The two variations correspond to the relations

$$\Phi_k(f^k) = Ku + \text{noise} \tag{10}$$

and

$$f^k = \Phi_k(Ku) + \text{noise} \tag{11}$$

where Φ_k represents the geometric distortion operator corresponding to the kth frame f^k.

2.1 Variation 1

The first model that we propose involves the relation

$$\Phi_k(f^k) = Ku + \text{noise}. \tag{12}$$

Using this relation, we propose the following minimization problem

$$\begin{aligned}\min_{v_1^k, v_2^k, u} \Big\{ E_1(u, v_1^k, v_2^k) \;&=\; \mu \sum_{k=1}^{\text{numFrames}} \int_\Omega (|\nabla v_1^k|^2 + |\nabla v_2^k|^2) dx \\ &+\; \lambda \sum_{k=1}^{\text{numFrames}} \int_\Omega (Ku - \Phi_k(f^k))^2 dx + \gamma \int_\Omega |\nabla u| dx \Big\},\end{aligned} \tag{13}$$

where f^k is the kth distorted frame of a true scene, K is the blur kernel, and Φ^k is the linear operator representing geometric distortions of the kth frame given by

$$\Phi_k(f^k(x_1, x_2)) = f^k(x_1 + v_1^k(x_1, x_2), x_2 + v_2^k(x_1, x_2)), \tag{14}$$

where each $v_1^k = v_1^k(x_1, x_2)$ and $v_2^k = v_2^k(x_1, x_2)$, and $v^k = (v_1^k, v_2^k)$ represents the turbulence warping from f^k to Ku.

The first term in E_1 is an H^1 regularization on v_1^k and v_2^k, which enforces a smooth turbulence warping. The second term in E_1 acts as a fidelity term that constrains the unknowns u, v_1^k and v_2^k to adhere to (12), and the last term in E_1 is simply the total variation (TV) regularization in u [14, 13], which allows for the restored image u to have edges.

To minimize the energy (14), we use Euler-Lagrange equations and alternating minimization in the unknowns. We give the associated gradient descent equations for u, v_1^k and v_2^k, where $k = 1, ..., \text{numFrames}$.

For u:

$$\frac{\partial u}{\partial t} = -\frac{\partial E_1}{\partial u} = \lambda \sum_{k=1}^{\text{numFrames}} \Big\{ -2K^*(Ku - \Phi_k(f^k)) \Big\} + \gamma \nabla \cdot \Big(\frac{\nabla u}{|\nabla u|} \Big).$$

For v_1^k:

$$\frac{\partial v_1^k}{\partial t} = -\frac{\partial E_1}{\partial v_1^k} = 2\mu \triangle v_1^k + 2\lambda (Ku - \Phi_k(f^k))(\Phi_k(f_x^k)).$$

For v_2^k:

$$\frac{\partial v_2^k}{\partial t} = -\frac{\partial E_1}{\partial v_2^k} = 2\mu \triangle v_2^k + 2\lambda(Ku - \Phi_k(f^k))(\Phi_k(f_y^k)).$$

The above equations are discretized using finite differences, and a fully explicit scheme is used to update the unknowns. We start with initial guess

$$u_0 = \text{constant} = \underset{(x_1,x_2)\in\Omega, k=1:\text{numFrames}}{\text{mean}} f^k(x_1, x_2)$$

and $v_1^k = v_2^k = 0$. We perform one iteration of gradient descent at each minimization step, using the previous u, v_1^k and v_2^k's in the update process. After updating each of the unknowns, the process is repeated until the energy E_1 reaches a steady state.

2.2 Variation 2

Similar to the first model, the second model that we propose involves the relation

$$f^k = \Phi_k(Ku) + \text{noise}. \tag{15}$$

With this relation, we propose the following minimization problem

$$\begin{aligned} \min_{v_1^k, v_2^k, u} \Big\{ E_2(u, v_1^k, v_2^k) \;&=\; \mu \sum_{k=1}^{\text{numFrames}} \int_\Omega (|\nabla v_1^k|^2 + |\nabla v_2^k|^2) dx \\ &+\; \lambda \sum_{k=1}^{\text{numFrames}} \int_\Omega (\Phi_k(Ku) - f^k)^2 dx + \gamma \int_\Omega |\nabla u| dx \Big\} \end{aligned} \tag{16}$$

where again f^k is the kth distorted frame of the true scene, K is the blur kernel, and Φ^k is the linear operator representing geometric distortions of the kth frame given by

$$\Phi_k((Ku)(x_1, x_2)) = (Ku)(x_1 + v_1^k(x_1, x_2), x_2 + v_2^k(x_1, x_2)), \tag{17}$$

where each $v_1^k = v_1^k(x_1, x_2)$ and $v_2^k = v_2^k(x_1, x_2)$, and $v^k = (v_1^k, v_2^k)$ represents the turbulence warping from Ku to f^k.

We use the same regularizations in v_1^k, v_2^k and u as in our first proposed model, and the only difference between this second model and the first is that the fidelity term reflects the relation (15).

To minimize (17), we again use Euler-Lagrange equations and alternating minimization. We give here the associated gradient descent equations for unknowns u, v_1^k and v_2^k, for $k = 1, ..., \text{numFrames}$.
For u:

$$\frac{\partial u}{\partial t} = -\frac{\partial E_2}{\partial u} = \lambda \sum_{k=1}^{\text{numFrames}} \Big\{ -2K^* \Phi_k^T (\Phi_k(Ku) - f^k) \Big\} + \gamma \nabla \cdot \left(\frac{\nabla u}{|\nabla u|} \right).$$

For v_1^k:

$$\frac{\partial v_1^k}{\partial t} = -\frac{\partial E_2}{\partial v_1^k} = 2\mu \triangle v_1^k - 2\lambda(\Phi_k(Ku) - f^k)(\Phi_k((Ku)_x))$$

For v_2^k:

$$\frac{\partial v_2^k}{\partial t} = -\frac{\partial E_2}{\partial v_2^k} = 2\mu \triangle v_2^k - 2\lambda(\Phi_k(Ku) - f^k)(\Phi_k((Ku)_y))$$

We discretize the above equations using finite differences, and using a fully explicit scheme, we update the unknowns. We start with initial guess

$$u_0 = \text{constant} = \underset{(x_1,x_2)\in\Omega, k=1:\text{numFrames}}{\text{mean}} f^k(x_1, x_2)$$

and $v_1^k = v_2^k = 0$. We perform one iteration of gradient descent at each minimization step, using previous u, v_1^k and v_2^k's in update process. After updating each of the unknowns, we repeat the process until the energy E_2 reaches a steady state.

3 Numerical Experiments

In this section, we provide some preliminary numerical results. We compare the results of our proposed variational model with the work found in [11] on geometric distortion correction and [8] on deconvolution using Fried kernel. In all examples, only 10 frames were used in the reconstructions.

As shown in [6], applying the temporal mean or median filter on the input frames often give a good reference image, with the temporal median producing a less blurred result than the temporal mean. In our results, we include the temporal mean and median of the input frames for comparison.

We begin with the simple case of $K = I$ where the blur kernel is simply the identity, representing the case of geometric distortion only and no blurring effects. The data was generated synthetically, and three sample frames of the geometric distortion are displayed to give the reader a sense of the magnitude of the distortion (top row of Fig. 1).

In the second case, we consider joint geometric distortion correction and deblurring, taking K to be the Fried kernel and look at the effect of the refractive index structure C_n^2 on the restored result. The data was collected by NATO SET156 (ex-SET072 RTG40) Group during the 2005 New Mexico's field trials. Three sample frames of each of the data sets are given (middle and bottom rows of Fig. 1).

3.1 Geometric Distortion Correction, Case: $K = I$

We begin by considering synthetic data that models turbulent geometric distortion without blur. The true image is 256×256, and we consider 10 distorted frames for our reconstructions. In Fig. 2, we present for comparison, the true image, the mean of the input frames, the median of the input frames, the geometric distortion corrected image using the algorithm in [11], and our restored results. Both Variation 1 and 2 of the proposed model corrects for the geometric distortion well, but the reconstructed images are not as sharp as the true image. The reconstruction using [11] is sharp, but fails to reconstruct parts of the image as well as our proposed model (e.g. the eyes). Furthermore, Variation 2 of our proposed model provides a sharper reconstruction than that of Variation 1. We would like to mention that the reconstructions using [11] utilize the nonlocal total variation regularization [5], and the

Figure 1: Three sample frames of distorted data.

reconstructions using our proposed model utilize the local total variation regularization. A more thorough comparison will be made in the future.

3.2 Joint Deblurring and Geometric Distortion Correction, K Fried Kernel

In this section, we present joint deblurring and geometric distortion correction numerical examples. We take K to be the Fried kernel. We consider two data sets (middle and bottom rows of Fig. 1). In both restorations, we use only 10 frames.

With the first example, we performed two restorations; one restoration uses the measured value of $C_n^2 = 1.51 \times 10^{-13}$ and the second uses the estimated $C_n^2 = 2.5 \times 10^{-13}$, which was found using the algorithm in [8]. Recall that a larger C_n^2 value creates a stronger blur kernel since it corresponds to higher levels of turbulence. Fig. 3 shows our joint deblurring and geometric distortion correction results along with a comparison with the geometrically

Figure 2: Geometric distortion correction. Top, left to right: true image, mean of 10 input frames, median of 10 input frames. Bottom, left to right: Variation 1 reconstruction, Variation 2 reconstruction, geometric distortion correction using [11].

corrected image using [11], and the deblurred results of the geometrically corrected image using [8] with Fried kernel corresponding to the two C_n^2 values. The second row of Fig. 3 corresponds to $C_n^2 = 1.51 \times 10^{-13}$. The restored images using Variation 1 and Variation 2 of our model are very similar; the result using Variation 2 is slightly sharper (see the lower part of the three bars farthest to the right). Whe n the larger estimated value of $C_n^2 = 2.5 \times 10^{-13}$ is used (see bottom row of Fig. 3), no difference can be detected between the restored images using Variation 1 and Variation 2. The restored images using first the geometric distortion correction [11] and then deconvolution with [8] give a more constant intensity along some of the bars (see the top of the bar second from the right) but overall are similar to the restored images using our proposed models.

With our second example, we performed restoration using the measured $C_n^2 = 1.91 \times 10^{-13}$ for our joint deblurring and geometric distortion correction models. Fig. 4 gives our restored images as well as a comparison with the geometrically corrected image using [11] and the blind deconvolution of this result using [8], where the approximated value of $C_n^2 = 1.7 \times 10^{-13}$. The restored images using our proposed models are similar, with Variation 2 giving a slightly sharper restored image (the top loop of the 'B' in 'ALBEDOS'). The result using [11] and [8] performs better in certain areas (the 'D' in 'ALBEDOS' looks nicer than in our restored images), but results using our model performs better in other areas (the 'A' and 'L' are more separated in 'ALBEDOS').

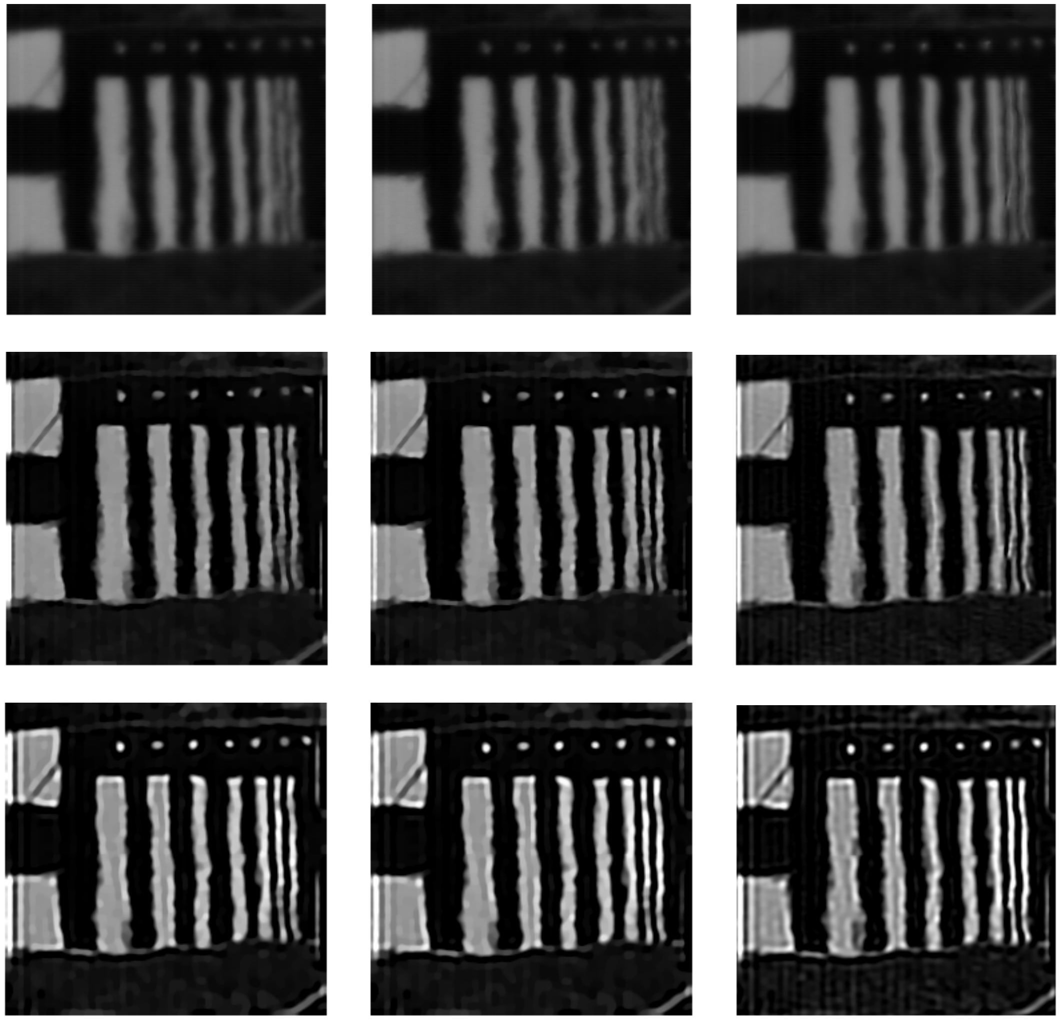

Figure 3: Top, left to right: mean of 10 input images, median of 10 input images, geometric distortion correction using [11]. Middle, left to right: reconstructions using Variation 1, Variation 2, and framelet non-blind deconvolution of geometrically corrected image (top right) using algorithm in [8]; here measured $C_n^2 = 1.51 \times 10^{-13}$ is used. Bottom, left to right: reconstructions using Variation 1, Variation 2, and blind deconvolution of geometrically corrected image (top right) using algorithm in [8]; here approximated value of $C_n^2 = 2.5 \times 10^{-13}$ is used.

4 Discussion

In the future, we will perform more numerical experiments to gain a better understanding of the performance of our proposed joint deblurring and geometric distortion correction models and to see if any improvements can be achieved using a combined model. For a more equal comparison with [11], we will implement the nonlocal total variation [5] in place of the total variation. In addition, to increase performance speed, we will utilize the Bregman iterative method [12].

Figure 4: Top, left to right: mean of 10 input images, median of 10 input images, geometrically restored image using [11]. Bottom, left to right: Variation 1 and Variation 2 reconstructions using measured $C_n^2 = 1.91 \times 10^{-13}$, blind Fried deconvolution of geometrically restored (top right) using [8] algorithm with estimated $C_n^2 = 1.7 \times 10^{-13}$.

References

[1] M. Aubailly, M.A. Vorontsov, G.W. Carhart, and M.T. Valley. Automated video enhancement from a stream of atmospherically-distorted images: the lucky-region fusion approach. *Proc. of SPIE*, 7463, 2009.

[2] D. Frakes, J. Monaco, and M. Smith. Suppression of atmospheric turbulence in video using an adaptive control grid interpolation approach. *IEEE International Conference on Acoustics, Speech, and Signal Processing*, 3:1881–1884, 2001.

[3] D.L. Fried. Optical resolution through a randomly inhomogeneous medium for very long and very short exposures. *Journal of The Optical Society of America*, 56:1372–1379, October 1966.

[4] S. Gepshtein, A. Shteinman, and B. Fishbain. Restoration of atmospheric turbulent video containing real motion using rank filtering and elastic image registration. *Proceedings of the Eusipco*, January 2004.

[5] G. Gilboa and S. Osher. Nonlocal operators with applications to image processing. *Multiscale Model Sim*, 7:1005–1028, 2008.

[6] J. Gilles. Restoration algorithm and system performance evaluation for active imaging systems. In *SPIE Europe Remote Sensing Conference*, Florence, Italy, September 2007.

[7] J. Gilles, T. Dagobert, and C.D. Franchis. Atmospheric turbulence restoration by diffeomorphic image registration and blind deconvolution. *Proceedings of the 10th International Conference on Advanced Concepts for Intelligent Vision Systems*, 2008.

[8] J. Gilles and S. Osher. Fried deconvolution. In *SPIE Defense, Security and Sensing conference*, Baltimore, US, April 2012.

[9] D. Li, R.M. Mersereau, and S. Simske. Atmospheric turbulence-degraded image restoration using principal component analysis. *IEEE Geoscience and Remote Sensing Letters*, 4:340–344, July 2007.

[10] Y. Lou, S.H. Kang, S. Soatto, and A.L. Bertozzi. Video stabilization of atmospheric turbulence distrotion. *UCLA C.A.M. Report 12-30*, April 2012.

[11] Y. Mao and J. Gilles. Non rigid geometric distortions correction - application to atmospheric turbulence stabilization. *to appear in Inverse Problems and Imaging*, 2012.

[12] S. Osher, M. Burger, D. Goldfarb, J. Xu, and W. Yin. An iterative regularization method for total variation-based image restoration. *Multiscale Model Sim*, 4(2):460–489, Jan 2005.

[13] L. Rudin and S. Osher. Total variation based image restoration with free local constraints. *Proc. IEEE ICIP*, 1:31–35, 1994.

[14] L.I. Rudin, S. Osher, and E. Fatemi. Nonlinear total variation based noise removal algorithms. *Physica D*, 60:259–268, 1992.

[15] M. Tahtali, A. Lambert, and D. Fraser. Self-tuning kalman filter estimation of atmospheric warp. *Proceedings of SPIE*, Jan 2008.

[16] A. Tunick, N. Tikhonov, M. Vorontsov, and G. Carhart. Characterization of optical turbulence (cn2) data measured at the arl a lot facility. *Army Research Lab, ARL-MR-625*, September 2005.